Dirac Fermions in Borophene

Baojie Feng,[1] Osamu Sugino,[1] Ro-Ya Liu,[1] Jin Zhang,[2] Ryu Yukawa,[3] Mitsuaki Kawamura,[1] Takushi Iimori,[1] Howon Kim,[1] Yukio Hasegawa,[1] Hui Li,[2] Lan Chen,[2] Kehui Wu,[2,4] Hiroshi Kumigashira,[3] Fumio Komori,[1] Tai-Chang Chiang,[5,1] Sheng Meng,[2,4] and Iwao Matsuda[1,*]

[1]*Institute for Solid State Physics, The University of Tokyo, Kashiwa, Chiba 277-8581, Japan*
[2]*Institute of Physics, Chinese Academy of Sciences, Beijing 100190, China*
[3]*Institute of Materials Structure Science, High Energy Accelerator Research Organization (KEK), Tsukuba, Ibaraki 305-0801, Japan*
[4]*Collaborative Innovation Center of Quantum Matter, Beijing 100871, China*
[5]*Department of Physics, University of Illinois, Urbana, Illinois 61801, USA*
(Received 24 September 2016; published 2 March 2017)

Honeycomb structures of group IV elements can host massless Dirac fermions with nontrivial Berry phases. Their potential for electronic applications has attracted great interest and spurred a broad search for new Dirac materials especially in monolayer structures. We present a detailed investigation of the β_{12} sheet, which is a borophene structure that can form spontaneously on a Ag(111) surface. Our tight-binding analysis revealed that the lattice of the β_{12} sheet could be decomposed into two triangular sublattices in a way similar to that for a honeycomb lattice, thereby hosting Dirac cones. Furthermore, each Dirac cone could be split by introducing periodic perturbations representing overlayer-substrate interactions. These unusual electronic structures were confirmed by angle-resolved photoemission spectroscopy and validated by first-principles calculations. Our results suggest monolayer boron as a new platform for realizing novel high-speed low-dissipation devices.

DOI: 10.1103/PhysRevLett.118.096401

Nontrivial lattice structures of solids involving more than one atom per lattice site can host novel properties and behaviors; hence, the discovery and design of new structure-property combinations are at the forefront of materials science. A celebrated, but particularly simple, example is the two-dimensional honeycomb lattice with just two atoms per unit cell [Fig. 1(a)], such as graphene [1,2], silicene [3–5], germanene [6,7], and stanene [8]. These materials can host Dirac cones (DC) that give rise to rich physical properties [2,9–11]. Recent theoretical investigations for new Dirac materials in simple two-dimensional structures have attracted great attention [12–16], whereas experimental observations of Dirac cones beyond the honeycomb structure are still rare.

A promising route for realizing novel two-dimensional materials is by tailoring or modifying the honeycomb lattice. An example is a monolayer boron sheet (i.e., borophene), which is realized by introducing periodic boron atoms in a honeycomblike lattice. As boron has one less electron than carbon, the honeycomb structure is unstable, but the introduction of additional boron atoms in the honeycomb lattice can stabilize the structures by balancing out the two- and multicenter bonds [17–19]. Depending on the arrangements of the extra boron atoms, various monolayer-boron structures have been proposed, such as the α sheet, β sheet, etc. [18–22]. Recently, several monolayer boron phases have been experimentally realized on Ag(111) [23–26]. For example, Mannix *et al.* reported a stable striped phase and a metastable homogeneous phase [23]. The striped phase was proposed to be a complete triangular lattice with anisotropic, out-of-plane buckling. In another study, a similar striped phase with a different rotation angle has been observed [25]. This phase, named a β_{12} sheet [Fig. 1(b)], has an essentially flat structure and interacts weakly with the Ag(111) substrate [25–28]. However, the experimental investigations on the electronic properties of monolayer boron are still rare.

In this Letter, we present a combined theoretical and experimental investigations on the β_{12} boron sheet. Our tight-binding analysis reveals that the lattice β_{12} sheet can

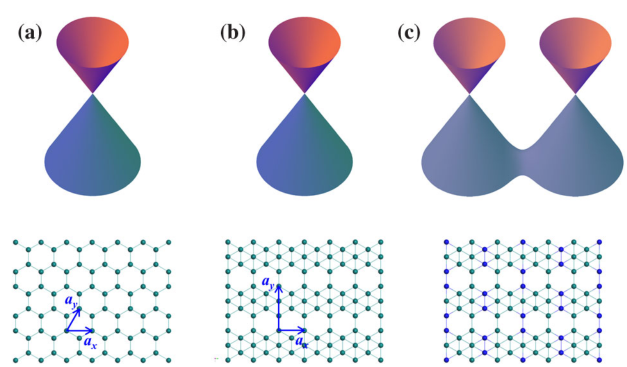

FIG. 1. Schematic drawing of the Dirac cones and lattices. (a) Honeycomb structure. (b) β_{12} sheet. (c) The β_{12} sheet with a 3×1 perturbation. The blue and green balls indicate the boron atoms with different on-site energies in our TB analysis. The top and bottom panels are the band structures and atomic structures, respectively. The basic vectors of the primitive unit cell are indicated by the blue arrows.

be decomposed into two triangular sublattices, analogous to the honeycomb lattice and, thus, hosts Dirac cones. Moreover, each Dirac cone can be split by introducing periodic perturbations representing the moiré pattern observed by a scanning tunneling microscope. These intriguing electronic structures have been confirmed by angle-resolved photoemission spectroscopy (ARPES) measurements and first-principles calculations. Our results have experimentally confirmed the first monolayer Dirac materials beyond the honeycomb structure and have validated a novel approach to split the Dirac cones by periodic perturbations. Moreover, these results suggest monolayer boron as a promising material for realizing high-speed, low-dissipation nanodevices.

In graphene, the π bands near the Fermi level (E_F), derived from the p_z orbital, form the Dirac cones at the K points [Fig. 1(a)] [2]. The s, p_x, and p_y orbitals are sp^2 hybridized and contribute to the σ bands which are far from E_F. The β_{12} sheet is also atomically flat, as is graphene, and, as confirmed later by our experiments and first-principles calculations, the bands near E_F are also derived from the p_z orbital. Interestingly, a simple tight-binding (TB) model, considering only the p_z orbital for a free-standing β_{12} sheet, shows the existence of Dirac cones centered at $(\pm 2\pi/3a, 0)$ in the first Brillouin zone (BZ), as illustrated in Fig. 1(b).

For a detailed understanding of the electronic structure of the system, we present the wave function for each boron atom in Fig. 2(a). Our TB analysis showed that the wave function at E_F has a vanishing amplitude at site c, owing to phase cancellation at the sixfold coordinated boron atoms. Instead, the wave function originates from the atoms at sites a, b, d, and e, which can be decomposed into two sublattices [Figs. 2(a) and 2(b)]. As a result, the equivalent structure of the β_{12} sheet is a honeycomb lattice, as shown in Fig. 2(c). As with graphene, this honeycomb lattice gives rise to a Dirac cone at each $\bar{K}$ point of the BZ. These Dirac cones are folded to $(\pm 2\pi/3a, 0)$, as illustrated in Fig. 2(d), because the B atoms at site c alter the shape and size of the BZ. The band structure from our TB calculations is shown in Fig. 2(e), where the two Dirac cones in the Γ-X axis are indicated by black arrows. For further confirmation, we also performed first-principles calculations for the free-standing β_{12} sheet, and the Dirac cones at $(\pm 2\pi/3a, 0)$ were reproduced [Fig. 2(f)]. The Dirac points were located at approximately 2 eV above the Fermi level, in agreement with previous reports [29]. The upward shift of the Dirac cones might originate from the electron deficiency of boron. It should be noted that the energy position of the Dirac points can be varied after being placed on a metal substrate to compensate for the electron deficiency [30].

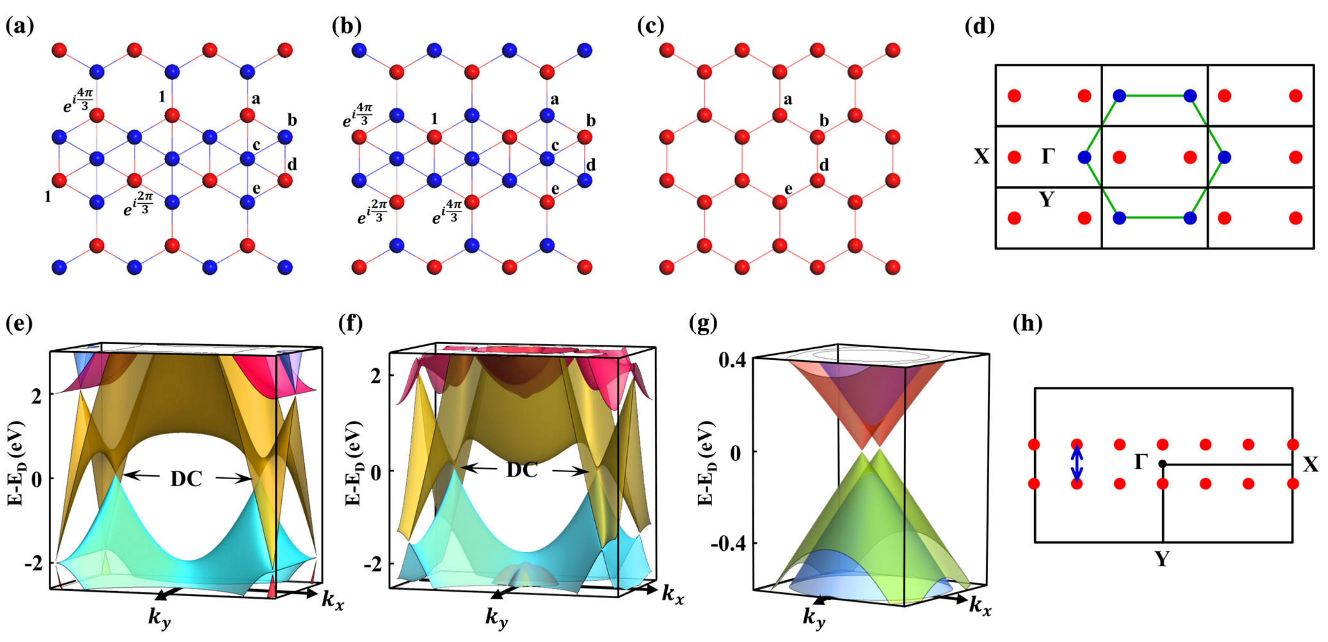

FIG. 2. TB model and first-principles calculations of the β_{12} sheet. (a) and (b) The wave function of each boron atom, as indicated by the amplitude near the red balls; the blue balls represent boron atoms with a vanishing amplitude. The boron atoms at site c always have a vanishing amplitude. The red balls are equivalent to the sublattices of the honeycomb lattice in (c). (d) Schematic drawing of the band folding process. The green hexagon and black rectangles indicate the BZ of the equivalent honeycomb lattice and the β_{12} sheet, respectively. The blue dots indicate the original Dirac cones (DC) from the honeycomb lattice; the red dots indicate the folded Dirac cones. (e) and (f) Band structures of free-standing β_{12} sheet from the TB model and first-principles calculations, respectively. E_D in the figure corresponds to the Dirac point, which is approximately 2 eV above the Fermi level from our first-principles calculations. The black arrows indicate the Dirac cones. (g) TB band structures of the β_{12} sheet under a modulated potential. The Dirac cone is split in the Γ-Y direction. (h) Schematic drawing of the folding and splitting (blue arrow) of the Dirac cones.

Similar Dirac cone states in a rectangular lattice have also recently been proposed in a graphene superlattice [45].

When the β_{12} sheet is placed on a Ag(111) substrate, a long-range modulation arising from the lattice mismatch gives rise to a moiré pattern, as shown in Fig. S4 [30]. As the interaction of the boron layer and Ag(111) substrate is weak, the β_{12} sheet remains largely intact and the moiré pattern can be explained by a modulated charge distribution on the surface [25]. The long-range modulation yields an electronic perturbation; in our TB model, we simulate this effect by varying the on-site energy over a superlattice period of $na_x \times ma_y$, where $a_x \times a_y$ is the original unit cell [Fig. 1(b)]. The Dirac cones of the superlattice are folded onto the Γ point when n is a multiple of three, and are further split into pairs in the Γ-Y direction when the sublattice symmetry is broken while retaining the inversion symmetry [Figs. 1(c) and 2(g)]. The Dirac cones will split in the Γ-X direction when the inversion symmetry is also broken [30]. The splitting of the Dirac cones has also been confirmed by our first-principles calculations considering the periodic perturbation [Fig. S2(b)]. From Fig. 2(g), the split Dirac cones are nonconcentric, which is different from the Rashba-type splitting of the Dirac cones in graphene [46,47].

To confirm these intriguing properties of the β_{12} sheet, we have performed high-resolution ARPES to directly measure its band structure. The sample was prepared by evaporating pure boron onto a Ag(111) substrate [30]. From LEED measurements [Fig. S4(a)], we found that there is only one phase, the β_{12} sheet. As the β_{12} sheet has a rectangular structure, different from the hexagonal structure of Ag(111), there exist domains with three equivalent orientations related by 120° rotations. A schematic drawing of the BZ of Ag(111) with the three domain orientations is shown in Fig. 3(a), together with the measured Fermi surface. Because the coverage of boron was less than one monolayer in the experiments, there were some areas of bare Ag(111) surface. As a result, the Shockley surface state and bulk sp band of Ag(111) were clearly observed,

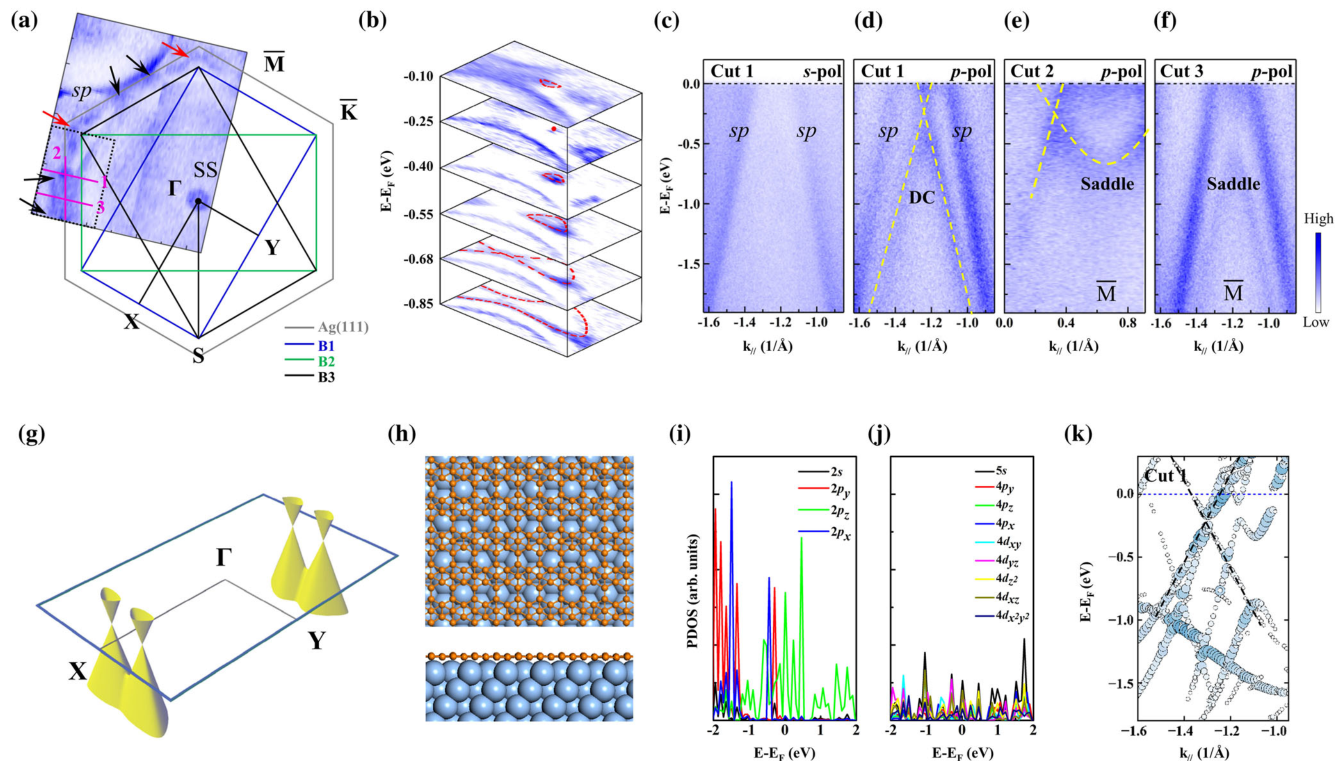

FIG. 3. Band structures of the β_{12} sheet on Ag(111). (a) The Fermi surface of the β_{12} sheet on Ag(111). The black, green, and blue rectangles indicate the BZ of three equivalent domains; the grey hexagon indicates the BZ of Ag(111). The black and red arrows indicate the bands of the boron layer. The surface state (SS) and bulk sp band of Ag(111) are also observed because the coverage of boron is less than 1 ML. The pink lines indicate cuts 1–3 where the ARPES intensity plots in (c)–(f) were measured. (b) CECs derived from the second-derivative energy distribution curves measured in the black dotted rectangle in (a). E_F in the figure corresponds to the Fermi level. All the data in (a) and (b) were measured with p polarized light. (c) ARPES intensity plot measured along cut 1 with s polarized light. (d)–(f) ARPES intensity plots measured with p polarized light along cut 1 to cut 3, respectively. The yellow dashed lines indicate the Dirac cones (DC). All the ARPES data in (a)–(f) were measured with a photon energy of 80 eV. (g) Schematic drawing of the Dirac cones according to our experimental results. (h) Relaxed structure model of the β_{12} sheet on Ag(111) from our first-principles calculations. The orange and blue balls indicate the B and Ag atoms, respectively. (i) and (j) Calculated PDOS of B atoms and Ag atoms, respectively. (k) Calculated band structure along cut 1.

as indicated by "SS" and "sp" in Fig. 3(a). The band structure from the boron layer shows one Fermi pocket centered at the S point of the β_{12} sheet and a pair of Fermi pockets centered at the $\bar{M}$ point of Ag(111), as indicated by the red and black arrows, respectively. The bands derived from the boron layer do not disperse with an increasing photon energy (Fig. S5), which is in agreement with its two-dimensional characteristic.

The pair of Fermi pockets centered at the $\bar{M}$ point of Ag(111) is associated with Dirac cones, in agreement with the general picture based on our calculations. In Fig. 3(b), we show constant energy contours (CECs) at different binding energies (E_B). With increasing binding energies, the Fermi pockets first shrink in size and then become points at $E_B = -0.25$ eV. Further increase of the binding energy leads to a pair of closed contours which touch each other at $E_B = -0.68$ eV. The pair of closed contours merges into one contour at higher binding energies.

The band structure measured along typical cuts in the momentum space [the pink lines in Fig. 3(a)] is shown in Figs. 3(c)–3(f). The measurements of cut 1 using p polarized light [Fig. 3(d)] reveal a Dirac cone as well as the bulk sp band of Ag(111). The Dirac point is located at approximately 0.25 eV below the Fermi level, in agreement with the evolution of the CECs in Fig. 3(b). The linear dispersing bands extend to as deep as 2 eV. Within our experimental resolution, there is no obvious energy gap at the Dirac point; thus, the quasiparticles are massless Dirac fermions. The Fermi velocities determined from Fig. 3(d) are approximately 6.1 and 7.0 eV · Å for the left and right branches of the Dirac cone, respectively, which are close to the Fermi velocity of graphene (~6.6 eV · Å). The slight difference of the Fermi velocity between the two branches originates from the anisotropy of the Dirac cones, in agreement with the CECs in Fig. 3(b). The neighboring bulk sp band of Ag(111) is clearly separated from the Dirac cone with no signs of hybridization, which indicates a weak interaction between the β_{12} sheet and the Ag(111) substrate, in agreement with previous work [28]. In Fig. 3(e), we show the band structure along the $\bar{K}$-$\bar{M}$-$\bar{K}$ direction; a pair of Dirac cones can be identified (indicated by the yellow dashed lines) although the one on the right side is only half visible because of the limitation of our experimental configuration. The two cones touch each other at the $\bar{M}$ point of Ag(111) at a binding energy of approximately 0.68 eV, which agrees with the evolution of the CECs discussed above. The band structure at the $\bar{M}$ point of Ag(111) shows a "V" shape along the $\bar{K}$-$\bar{M}$-$\bar{K}$ direction [Fig. 3(e)] and a "Λ" shape along the $\bar{\Gamma}$-$\bar{M}$ direction [Fig. 3(f)]; the bottom of the V and the top of the Λ are located at the same binding energy (~0.68 eV), which suggests a "saddle" point at the $\bar{M}$ point of Ag(111). Within the first BZ of the β_{12} sheet, we observed two pairs of Dirac cones in total, as schematically illustrated in Fig. 3(g).

The orbital contribution of the boron bands can be probed by switching the linear polarization of the incident light. The s polarized light primarily probes the in-plane p_x and p_y orbitals, while the p polarized light probes both the in-plane (p_x and p_y) and out-of-plane (p_z) orbitals. The band structures along cut 1 measured with s and p polarized light are shown in Figs. 3(c) and 3(d), respectively. The Dirac cone was not observed with the s polarized light, leaving only the bulk sp bands of Ag(111). This means that the Dirac cones originate from the p_z orbital of boron. For further confirmation, we performed first-principles calculations for the B/Ag(111) system. The relaxed atomic structure shown in Fig. 3(h) agrees with previous work [25]. The partial density of states (PDOS) of the boron and silver atoms is shown in Figs. 3(i) and 3(j). Near E_F, the DOS is mainly derived from the p_z orbital of boron; the contributions from the p_x and p_y orbitals of boron are essentially negligible [Fig. 3(i)]. Likewise, the contributions from Ag orbitals are much smaller compared with those from the p_z orbital of boron [Fig. 3(j)]. We conclude that the Dirac cones are predominantly derived from the p_z orbital of boron, with little hybridization with the Ag substrate states. This observation validates our TB analysis in terms of the boron p_z orbital only.

Although the contributions from the Ag atoms is much smaller than the p_z orbital of boron, there are still considerable contributions from the 5 s, $4d_{z^2}$, $4d_{xz}$, and $4d_{yz}$ orbitals of Ag atoms over much of the valence band range. These orbitals have large out-of-plane components and could potentially hybridize with the p_z orbital of boron, which can explain the origin of the weak interaction between the β_{12} sheet and the Ag(111) substrate. This interaction might energetically shift the bands of the free-standing β_{12} sheet, moving the Dirac points below the Fermi level. Another important consequence of this interaction is the appearance of the moiré pattern. From Fig. S4(b), the period of the moiré pattern is approximately $5.5a_x$, which is approximately two times the period of the perturbation in our TB model [Fig. 1(c)]. This observation validates our qualitative explanation for the splitting of the Dirac cones. Alternatively, the splitting of the Dirac cones could be interpreted in terms of a uniaxial strain in the β_{12} sheet associated with the moiré pattern. The strain in the lattice could break the equivalence of bonds, inducing a splitting of the π bands [45]. The net results would be similar to those caused by a modulation of the on-site energy. On the other hand, owing to the existence of the moiré pattern, the pair of Dirac cones centered at $(\pm 2\pi/3a, 0)$ of the β_{12} sheet are folded to the $\bar{M}$ point of Ag(111), in agreement with our experiments. As a further test of our explanation, first-principles calculations of B/Ag(111) also reveal the same pair of Dirac cones, as shown in Fig. 3(k). The calculated Fermi velocity is approximately 3.5 eV · Å, which is in the same order of magnitude as the experimental value. The difference between the theoretical and experimental results might originate from the many-body interactions, which have already been extensively studied in graphene [48,49].

All of our results support or confirm the existence of gapless Dirac cones in the β_{12} boron sheet grown on Ag(111). These Dirac cones are split into pairs owing to the interaction of the boron layer with the substrate. An important implication of our analysis and discussion of the underlying physics is that Dirac cone features can arise in lattices with large unit cells; such systems tend to exhibit multiple motifs and are conducive to atomic scale engineering of the structure. Our work suggests opportunities and strategies in connection with the realization of Dirac and, possibly, other exotic phases; it might also stimulate further investigation of the novel properties of monolayer boron, such as superconductivity [29], topological order, and high-speed electronic transport and switching.

We thank Professor X. J. Zhou for providing the Igor macro to analyze the ARPES data. The ARPES measurement was performed at Photon Factory, KEK under the approval of the Program Advisory Committee (Proposals 2015S2-005 and 2016G602) at the Institute of Materials Structure Science at KEK. This work was supported by the Synchrotron Radiation Research Organization at the University of Tokyo, the Ministry of Education, Culture, Sports, Science and Technology of Japan (Photon and Quantum Basic Research Coordinated Development Program), the Japan Society for the Promotion of Science (JSPS) grant-in-aid for specially promoting research (Grant No. 23000008), the JSPS grant-in-aid for Scientific Research (B) (Grant No. 26287061), Japan Science and Technology Agency (JST) ACT-C, the U.S. National Science Foundation (Grant No. DMR-1305583), the Ministry of Science and Technology of the People's Republic of China (MOST) (Grants No. 2013CB921702, No. 2013CBA01601, No. 2016YFA0202301, No. 2016YFA0300902), the National Natural Science Foundation of China (Grants No. 11322431, No. 1674366, No. 11334011), and the Strategic Priority Research Program of the Chinese Academy of Sciences (Grant No. XDB07020100).

*imatsuda@issp.u-tokyo.ac.jp

[1] A. K. Geim and K. S. Novoselov, Nat. Mater. **6**, 183 (2007).
[2] A. H. Castro Neto, F. Guinea, N. M. R. Peres, K. S. Novoselov, and A. K. Geim, Rev. Mod. Phys. **81**, 109 (2009).
[3] M. Houssa, A. Dimoulas, and A. Molle, J. Phys. Condens. Matter **27**, 253002 (2015).
[4] J. Zhuang, X. Xu, H. Feng, Z. Li, X. Wang, and Y. Du, Sci. Bull. **60**, 1551 (2015).
[5] J. Zhao, H. Liu, Z. Yu, R. Quhe, S. Zhou, Y. Wang, C. C. Liu, H. Zhong, N. Han, J. Lu, Y. Yao, and K. Wu, Prog. Mater. Sci. **83**, 24 (2016).
[6] L. Li, S.-z. Lu, J. Pan, Z. Qin, Y.-q. Wang, Y. Wang, G.-y. Cao, S. Du, and H.-J. Gao, Adv. Mater. **26**, 4820 (2014).
[7] M. Derivaz, D. Dentel, R. Stephan, M.-C. Hanf, A. Mehdaoui, P. Sonnet, and C. Pirri, Nano Lett. **15**, 2510 (2015).
[8] F. Zhu, W. Chen, Y. Xu, C. Gao, D. Guan, C. Liu, D. Qian, S.-C. Zhang, and J. Jia, Nat. Mater. **14**, 1020 (2015).
[9] B. Feng, H. Li, C.-C.Liu, T.-N. Shao, P. Cheng, Y. Yao, S. Meng, L. Chen, and K. Wu, ACS Nano **7**, 9049 (2013).
[10] M. Ezawa, Phys. Rev. Lett. **109**, 055502 (2012).
[11] Y. Xu, B. Yan, H.-J. Zhang, J. Wang, G. Xu, P. Tang, W. Duan, and S.-C. Zhang, Phys. Rev. Lett. **111**, 136804 (2013).
[12] D. Malko, C. Neiss, F. Viñes, and A. Görling, Phys. Rev. Lett. **108**, 086804 (2012).
[13] L. Z. Zhang, Z. F. Wang, Z. M. Wang, S. X. Du, H.-J. Gao, and F. Liu, J. Phys. Chem. Lett. **6**, 2959 (2015).
[14] J. Wang, S. Deng, Z. Liu, and Z. Liu, Natl. Sci. Rev. **2**, 22 (2015).
[15] G. van Miert and C. M. Smith, Phys. Rev. B **93**, 035401 (2016).
[16] X.-F. Zhou, X. Dong, A. R. Oganov, Q. Zhu, Y. Tian, and H.-T. Wang, Phys. Rev. Lett. **112**, 085502 (2014).
[17] M. H. Evans, J. D. Joannopoulos, and S. T. Pantelides, Phys. Rev. B **72**, 045434 (2005).
[18] H. Tang and S. Ismail-Beigi, Phys. Rev. B **82**, 115412 (2010).
[19] H. Tang and S. Ismail-Beigi, Phys. Rev. Lett. **99**, 115501 (2007).
[20] X. Wu, J. Dai, Y. Zhao, Z. Zhuo, J. Yang, and X. C. Zeng, ACS Nano **6**, 7443 (2012).
[21] E. S. Penev, S. Bhowmick, A. Sadrzadeh, and B. I. Yakobson, Nano Lett. **12**, 2441 (2012).
[22] H. Liu, J. Gao, and J. Zhao, Sci. Rep. **3**, 3238 (2013).
[23] A. J. Mannix, X.-F. Zhou, B. Kiraly, J. D. Wood, D. Alducin, B. D. Myers, X. Liu, B. L. Fisher, U. Santiago, J. R. Guest, M. J. Yacaman, A. Ponce, A. R. Oganov, M. C. Hersam, and N. P. Guisinger, Science **350**, 1513 (2015).
[24] Z. Zhang, E. S. Penev, and B. I. Yakobson, Nat. Chem. **8**, 525 (2016).
[25] B. Feng, J. Zhang, Q. Zhong, W. Li, S. Li, H. Li, P. Cheng, S. Meng, L. Chen, and K. Wu, Nat. Chem. **8**, 563 (2016).
[26] B. Feng, J. Zhang, R.-Y. Liu, T. Iimori, C. Lian, H. Li, L. Chen, K. Wu, S. Meng, F. Komori, and I. Matsuda, Phys. Rev. B **94**, 041408(R) (2016).
[27] Y. Liu, E. S. Penev, and B. I. Yakobson, Angew. Chem., Int. Ed. **52**, 3156 (2013).
[28] Z. Zhang, Y. Yang, G. Guo, and B. I. Yakobson, Angew. Chem. Int. Ed. **54**, 13022 (2015).
[29] E. S. Penev, A. Kutana, and B. I. Yakobson, Nano Lett. **16**, 2522 (2016).
[30] See Supplemental Material at http://link.aps.org/supplemental/10.1103/PhysRevLett.118.096401 for details of the TB analysis and sample characterization, which includes Refs. [31–44].
[31] P. Giannozzi *et al.*, J. Phys. Condens. Matter **21**, 395502 (2009).
[32] The ELK FP-LAPW Code. http://elk.sourceforge.net.
[33] T. Ozaki, Phys. Rev. B **67**, 155108 (2003).
[34] D. Vanderbilt, Phys. Rev. B **41**, 7892(R) (1990).

[35] E. Kucukbenli, M. Monni, B. I. Adetunji, X. Ge, G. A. Adebayo, N. Marzari, S. de Gironcoli, and A. D. Corso, arXiv:1404.3015.
[36] T. Ozaki and H. Kino, Phys. Rev. B **69**, 195113 (2004).
[37] A. A. Mostofi, J. R. Yates, G. Pizzi, Y.-S. Lee, I. Souza, D. Vanderbilt, and N. Marzari, Comput. Phys. Commun. **185**, 2309 (2014).
[38] A. Bostwich, T. Ohta, T. Seyller, K. Horn, and E. Rotenberg, Nat. Phys. **3**, 36 (2007).
[39] I. Gierz, J. Henk, H. Höchst, C. R. Ast, and K. Kern, Phys. Rev. B **83**, 121408 (2011).
[40] G. Kresse and J. Furthmüller, Phys. Rev. B **54**, 11169 (1996).
[41] P. E. Blöchl, Phys. Rev. B **50**, 17953 (1994).
[42] H. J. Monkhorst and J. D. Pack, Phys. Rev. B **13**, 5188 (1976).
[43] P. V. C. Medeiros, S. Stafström, and J. Björk, Phys. Rev. B **89**, 041407(R) (2014).
[44] P. V. C. Medeiros, S. S. Tsirkin, S. Stafström, and J. Björk, Phys. Rev. B **91**, 041116(R) (2015).
[45] T.-T. Jia, M.-M. Zheng, X.-Y. Fan, Y. Sun, S.-J. Li, H.-Y. Liu, G. Chen, and Y. Kawazoe, Sci. Rep. **6**, 18869 (2016).
[46] A. Varykhalov, J. Sanchez-Barriga, A. M. Shikin, C. Biswas, E. Vescovo, A. Rybkin, D. Marchenko, and O. Rader, Phys. Rev. Lett. **101**, 157601 (2008).
[47] D. Marchenko, A. Varykhalov, M. R. Scholz, G. Bihlmayer, E. I. Rashba, A. Rybkin, A. M. Shikin, and O. Rader, Nat. Commun. **3**, 1232 (2012).
[48] D. C. Elias, R. V. Gorbachev, A. S. Mayorov, S. V. Morozov, A. A. Zhukov, P. Blake, L. A. Ponomarenko, I. V. Grigorieva, K. S. Novoselov, F. Guinea, and A. K. Geim, Nat. Phys. **7**, 701 (2011).
[49] C. Hwang, D. A. Siegel, S.-K. Mo, W. Regan, A. Ismach, Y. Zhang, A. Zettl, and A. Lanzara, Sci. Rep. **2**, 590 (2012).